

## Article

# Microstructure and Mechanical Properties Investigation of the CoCrFeNiNb<sub>x</sub> High Entropy Alloy Coatings

Hui Jiang <sup>1</sup>, Kaiming Han <sup>1,\*</sup>, Dayan Li <sup>2</sup> and Zhiqiang Cao <sup>2</sup>

<sup>1</sup> College of Mechanical and Electronic Engineering, Shandong University of Science and Technology, Qingdao 266590, China; jianghui2013@mail.dlut.edu.cn

<sup>2</sup> Key Laboratory of Solidification Control and Digital Preparation Technology (Liaoning Province), School of Materials Science and Engineering, Dalian University of Technology, Dalian 116024, China; songlijiao94@163.com (D.L.); caozq@dlut.edu.cn (Z.C.)

\* Correspondence: hankaiming@126.com; Tel.: +86-411-8470-6169

Received: 23 September 2018; Accepted: 23 October 2018; Published: 31 October 2018



**Abstract:** In this work, the CoCrFeNiNb<sub>x</sub> ( $x$ : molar ratio,  $x = 0.45, 0.5, 0.75$ , and  $1.0$ ) high entropy alloy coatings were synthesized on a 304 stainless steel substrate by laser cladding to investigate the effect of Nb element on their microstructure, hardness, and wear resistance. The results indicated that in all of the CoCrFeNiNb<sub>x</sub> alloy coatings, two phases were found: One was a face-centered cubic (FCC) solid solution phase, the other was a Co<sub>1.92</sub>Nb<sub>1.08</sub>-type Laves phase. The microstructures of samples varied from hypoeutectic structure ( $x = 0.45$  and  $0.5$ ) to hypereutectic structure ( $x = 0.75$  and  $1.0$ ). The Vickers hardness of CoCrFeNiNb<sub>x</sub> alloy coatings was obviously improved compared with the substrate. The hardness value of the CoCrFeNiNb<sub>1.0</sub> alloy coating reached to 590 HV, which was 2.8 times higher than that of the substrate. There was also a corresponding variation in wear properties with hardness evolutions. Wherein the hypereutectic CoCrFeNiNb<sub>1.0</sub> alloy coating with the highest hardness exhibited the best wear resistance under the same wear condition, the dry wear test showed the wear mass loss of CoCrFeNiNb<sub>1.0</sub> alloy coating was less than a third of the substrate. The high hardness and wear resistance properties were considered with the fine lamellar eutectic structure and proper combination of FCC and Laves phases.

**Keywords:** high entropy alloy coating; eutectic microstructure; Vickers hardness; wear property

## 1. Introduction

Conventional alloys are mainly based on one or two principal elements with the addition of several minor elements to improve the properties. Different from the conventional alloy design, high entropy alloys (HEAs) or multi-principal element alloys are designed based on several components (usually containing at least five elements) with concentrations between 5 to 35 at. % [1–4]. It was historically assumed that the presence of a high concentration of multiple alloying elements would embrittle material by forming intermetallic compounds. However, previous studies showed that HEAs tended to form a simple solution phase, which attributed to a high entropy effect. For example, the CoCrFeNiMn [2,5] alloy exhibits a single FCC phase. The WMoNbTa, WMoNbTaV, TiZrHfNbMo, TaNbZrHf, and TiZrHfNbTa refractory HEAs [6–9] are composed of a single body centered cubic (BCC) phase. The GdHoLaTbY, Ho-Dy-Y-Gd-Tb, YGdTbDyLu, and GdTbDyTmLu HEAs [10–12] are composed of a hexagonal close-packed (HCP) phase. The Ti<sub>35</sub>Zr<sub>27.5</sub>Nb<sub>5</sub>Hf<sub>27.5</sub>Ta<sub>5</sub> alloy [13] has a peculiar single orthorhombic phase. More importantly, HEAs show attractive physical and mechanical properties because of their unique structure, such as high strength/hardness [14–16], excellent wear resistance [17–19], high-temperature stability [20,21], corrosion resistance [22,23],

superconductivity [24,25], soft magnetism [26,27], etc. As a result, HEAs can be an attractive material for a range of applications. However, the cost of HEAs is higher than that of conventional alloys because of the expensive high-purity raw materials. To reduce the cost, the HEA coatings obtained by laser cladding with advanced properties continue to be in great demand. At present, laser cladding as a surface coating method has been the subject of extensive research [28,29]. Advantages of laser cladding are the integrity of the fusion bond between the cladding coating and substrate, smaller thermal effects on the substrate, high process flexibility, high working speeds, and environmental protection. Moreover, the rapid solidification of laser cladding results in the finer microstructure and extended solid solution, in addition to the high-performance surface with enhanced properties. Stainless steels are widely used in industry and daily life due to their high corrosion, oxidation resistance, and workability. However, its low hardness and wear resistance are not ideal for practical applications. Therefore, the enhancement of hardness and wear resistance of the 304 stainless steels is quite necessary. Recently, there has been a growing interest in the fabrication of surface layers of HEAs on stainless steel [30–32]. The hardness and wear resistance of stainless steel can be improved by coating HEA on its surface. For example, FeCoCrAlNi HEA coating [33] prepared by laser cladding on 304 stainless steel possessed high hardness, which was ~three times higher than that of the substrate. FeNiCoSiCrAlTi HEA coating [34] prepared by laser cladding on Q235 steel showed a much higher hardness ( $\approx 780 \text{ HV}_{0.5}$ ).

In our previous work, the microstructure and mechanical properties of CoCrFeNiNb<sub>x</sub> eutectic high entropy alloy (EHEA system [35] prepared by vacuum arc melting were well investigated. Results indicated that the microstructure changed from a hypoeutectic structure ( $x < 0.45$ ) to eutectic structure with FCC + Laves dual-phase at  $x = 0.45$ , and then to hypereutectic structure ( $x > 0.45$ ). In addition, the CoCrFeNiNb<sub>x</sub> HEAs ( $x \geq 0.45$ ) represented a relatively high hardness and wear resistance properties. In this paper, the CoCrFeNiNb<sub>x</sub> ( $x \geq 0.45$ ) HEA coatings on 304 stainless steel substrate were prepared by laser cladding to investigate the effect of Nb element on their microstructure, hardness, and wear resistance.

## 2. Experimental Details

The substrate material was 304 Stainless steel with a size of 25 mm × 15 mm × 5 mm. The substrate surface was polished using 1000# sandpaper. Then the surface was washed using ethylalcohol and dried. The Co, Cr, Fe, Ni, and Nb alloy powders were used for laser cladding CoCrFeNiNb<sub>x</sub> ( $x$  value in molar ratio,  $x = 0.45, 0.5, 0.75$ , and  $1.0$ , denoted as Nb0.45, Nb0.5, Nb0.75, and Nb1.0, respectively) HEA coatings. These alloy powders were thoroughly mixed for 1 h and dried in a vacuum oven for 2 h prior to the experiment. The prepared alloy powders were placed on the surface of 304 stainless steel to form a powder bed with a thickness of 1.2 mm. In laser cladding, the CoCrFeNiNb<sub>x</sub> HEA coatings were performed using a laser processing machine (LWS-500 Laserline, Koblenz, Germany) with the high-purity argon supplied to prevent oxidation. The laser power of 1000 W, spot diameter ( $D$ ) of 4 mm, and scanning speed ( $V$ ) of 6 mm/s were used in the experiment (in this paper, these processing parameters for laser cladding are optimized to obtain good quality alloy coatings).

After the laser cladding process, the coatings were cut in the plane perpendicular to the laser tracks using electro-spark wire-electrode cutting. The cross-section of HEA coating was subjected to a usual metallographic procedure, followed by polishing, and then etched with alcoholic dilute aqua regia solution. The crystallographic structure of the coatings was characterized by a Bruker D8 X-ray diffractometer (XRD, Bruker, Ettlingen, Germany) with the Cu K $\alpha$  radiation ( $\lambda = 0.15406 \text{ nm}$ ) at a scanning speed of  $4^\circ/\text{min}$ , and a  $2\theta$  scattering range of  $20$  to  $100^\circ$ . The cross-section microstructures of samples were observed by Zeiss Supra 55 scanning-electron microscopy (SEM, Zeiss, Oberkochen, Germany) with energy dispersive spectrometry (EDS) utilized to analyze the chemical compositions of different regions. The micro-hardness of the coatings was measured by an Vickers hardness tester (Yante, Shanghai, China) with a load of 500 g and loading time of 15 s. The interval of each point was kept at  $100 \mu\text{m}$  and five points were measured for each position and then the average hardness was used in this paper.

The longitudinal-section of coatings used in the wear and abrasion test was prepared in an epoxy mount and polished. The wear resistance performance of the coatings was investigated by a computer-controlled ball-on-disc wear tester (CFT-I, Zhongke Kaihua, Lanzhou, China) under dry sliding conditions. The sliding mode was reciprocating sliding, and the oscillating stroke was 5 mm. Silicon nitride ball with a diameter of 3 mm was selected as a counterpart. The applied load was 15 N and the test time was 60 min. The weight loss during wear test was measured using an electric balance with a resolution of 0.1 mg and average weight loss values of five times for each specimen were used in this paper. After the wear resistance test, wear scar width and depth were measured by a confocal laser scanning microscope (LEXT OLS4000, Olympus, Tokyo, Japan); ten sets of data were measured and an average value was taken as the final result. Worn surfaces were analyzed using a LEXT and SEM with EDS.

### 3. Results and Discussion

#### 3.1. Constituent Phases

The XRD patterns of the CoCrFeNiNb<sub>x</sub> HEA coatings are shown in Figure 1. It could be observed that there were two phases, one was an FCC solid solution phase, the other was a Co<sub>1.92</sub>Nb<sub>1.08</sub>-type Laves phase in all of Nb0.45, Nb0.5, Nb0.75, and Nb1.0 HEA coatings, which was consistent with the alloys prepared by arc melting [35]. Moreover, the strength of the Laves phase diffraction peaks increased with increasing Nb content, indicating that the volume fraction of the Laves phase increased.

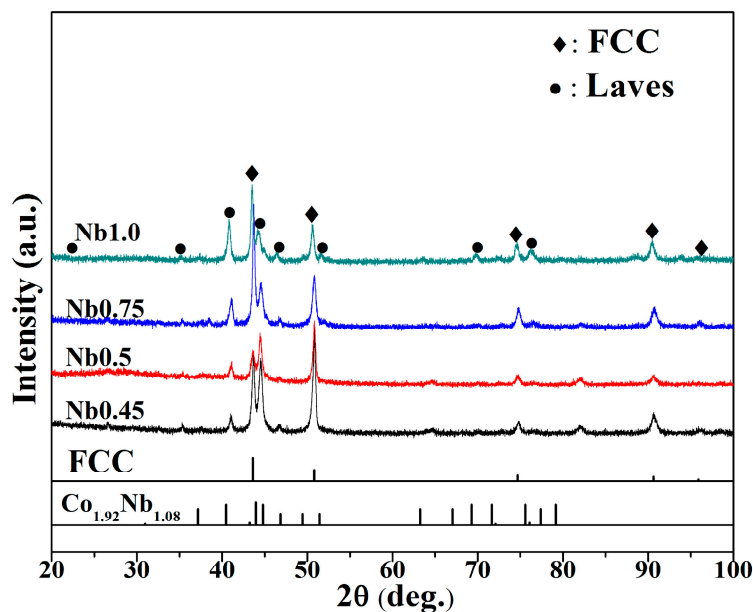


**Figure 1.** X-ray diffractometer patterns of the CoCrFeNiNb<sub>x</sub> high entropy alloys (HEA) coatings.

To date, certain methods, such as thermodynamic modeling and empirical or semi-empirical parameters, for the prediction of the phase composition of HEAs have been developed. The parameters of atomic size difference ( $\Delta\delta$ ), valence electron concentration (VEC), Pauling electronegativity difference ( $\Delta\chi_{\text{Pauling}}$ ), enthalpy of mixing ( $\Delta H_{\text{mix}}$ ),  $\gamma$  ( $\gamma = \omega_s/\omega_L$ ), where  $\omega_s$  and  $\omega_L$  are the solid angles of the smallest and largest atoms, respectively, were used to predict the formation between a simple solid solution and intermetallic phases [36–40]. In this section, these parameters of  $\Delta\delta$ ,  $\Delta H_{\text{mix}}$ ,  $\Delta\chi_{\text{Pauling}}$ ,  $\gamma$ , and VEC were calculated and results were listed in Table 1. The calculation formulas for  $\Delta\delta$ ,  $\Delta H_{\text{mix}}$ ,  $\Delta\chi_{\text{Pauling}}$ ,  $\gamma$ , and VEC can be obtained from [36–39]. In Table 1, it is noted that the values of  $\Delta\delta$  in all CoCrFeNiNb<sub>x</sub> HEA coatings with an FCC phase and Laves phase were over 4.27%, which matches with Jiang’s prediction [36]. VEC is critical in predicting the type of simple solid solution phase in HEAs. FCC solid-solution phases are stable at higher VEC ( $\geq 8$ ), while BCC solid-solution

phases are stable at lower VEC (<6.8). The VEC values of all the studied HEA coatings change from 7.92 to 7.6, and, therefore, tend to form an FCC phase in accordance with the prediction [37]. A Laves phase forms in the  $\text{CoCrFeNiNb}_x$  ( $x \geq 0.45$ ) HEAs with  $\Delta\chi_{\text{pauling}} \leq 0.123$ , which is inconsistent with the criterion  $\Delta\chi_{\text{pauling}} > 0.133$  for topologically closepacked phase (TCP) phase formation [39]. However, the  $\gamma$  values of  $\text{CoCrFeNiNb}_x$  HEA coatings are higher than 1.175. This is in agreement with Wang's prediction, which suggests that most of the multi phases with intermetallics are distributed in the region of  $\gamma > 1.175$  in HEAs [38]. It should be noted that using a sole parameter cannot accurately predict the phase composition in the HEAs, so the comprehensive effect of all these parameters needs to be considered.

**Table 1.** The parameters of  $\Delta\delta$ ,  $\Delta H_{\text{mix}}$ ,  $\Delta\chi_{\text{pauling}}$ ,  $\gamma$ , and valence electron concentration (VEC) for the  $\text{CoCrFeNiNb}_x$  HEA coatings.

Alloys	$\Delta\delta$ (%)	$\Delta H_{\text{mix}}$ (KJ/mol)	$\gamma$	$\Delta\chi_{\text{pauling}}$	VEC
$\text{CoCrFeNiNb}_{0.45}$	4.9	−10.12	1.197	0.1132	7.92
$\text{CoCrFeNiNb}_{0.5}$	5.09	−10.667	1.197	0.1144	7.89
$\text{CoCrFeNiNb}_{0.75}$	5.82	−13.03	1.196	0.1196	7.74
$\text{CoCrFeNiNb}_{1.0}$	6.32	−14.88	1.195	0.1234	7.6

### 3.2. Microstructures

Figure 2 exhibits typical macroscopic morphologies in the cross-section of the HEA coatings. From Figure 2a, it could be found that the coating had good geometry, being uniform and free of cracks and porosity. In addition, no clear boundary existed between the substrate and cladding coating, see Figure 2b, which indicated an excellent metallurgical bonding between the coating and the substrate. The sample could be divided into two parts of coatings, consisting of the cladding zone (denoted as CZ) and the heat-affected zone (denoted as HAZ) from bottom to top.

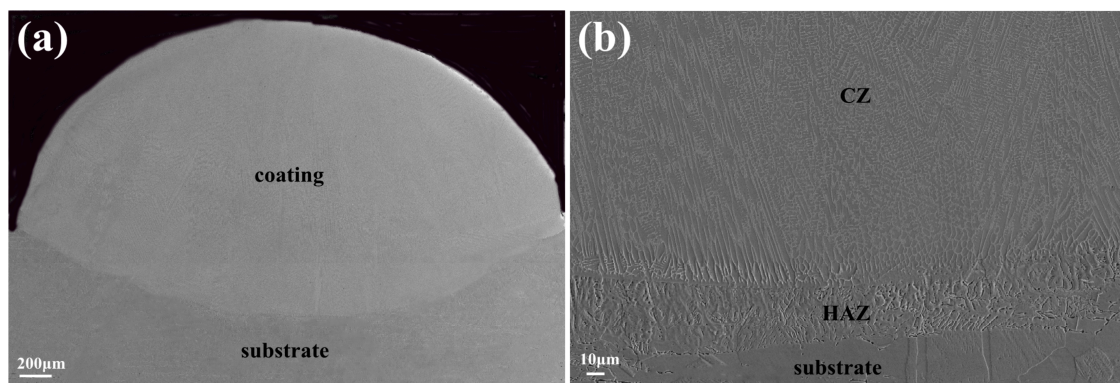


**Figure 2.** The typical macroscopic morphology in the cross-section of the HEA coating (a) overall morphology, (b) cross-sectional view.

To investigate the microstructures of the  $\text{CoCrFeNiNb}_x$  HEA coatings, the images of the central area in the cladding zone of  $\text{CoCrFeNiNb}_x$  HEA coatings are given, as shown in Figure 3. The  $\text{Nb}_{0.45}$  and  $\text{Nb}_{0.5}$  alloy coatings presented a typical dendritic morphology, in which the interdendritic region consisted of a lamellar eutectic structure (denoted as E). This indicated that the  $\text{Nb}_{0.45}$  and  $\text{Nb}_{0.5}$  alloy coatings were hypoeutectic alloys with a primary  $\alpha$  phase. However, in arc melting, a full eutectic structure was obtained in the  $\text{Nb}_{0.45}$  alloy and a hypereutectic structure was found in the  $\text{Nb}_{0.5}$  alloy. It is possible that the cooling rate and the solidification velocity of the laser cladding sample were higher than that of the arc melting sample which did not allow the growth of secondary dendrites. In order to investigate the other reasons, the chemical compositions in different regions were measured by EDS and are listed in Table 2. The results showed that the Fe content in these coatings was higher than that in the designed alloy composition. The reason was that Fe could diffuse



from the 304 stainless steel substrate into the HEA coating during laser cladding. The high Fe content in the HEA coatings may be the main reason that the Nb0.45 and Nb0.5 alloy coatings possessed a hypoeutectic structure. To verify the assumption, the enhanced Fe content CoCrFe<sub>2</sub>NiNb<sub>0.5</sub> alloy (denoted as Fe2Nb0.5) was prepared by arc melting, see Figure 3e, and the results showed that the alloy displayed a typical hypoeutectic structure. This demonstrated the higher Fe content in the Nb0.45 and Nb0.5 alloy coatings enhanced the solid solubility of Nb, thereby leading to the extension of the eutectic composition point to a higher Nb content. For Nb0.75 and Nb1.0 alloy coatings, the primary phase changed to the  $\beta$ -phase, this indicated that these samples were hypereutectic. As listed in Table 2, in hypoeutectic Nb0.45 and Nb0.5 alloy coatings, the eutectic region was enriched in Nb, while the primary  $\alpha$ -phase was depleted in Nb element and the primary  $\beta$ -phase contained more Nb element relative to the eutectic region. Based on the XRD and EDS analysis results, it was plausible to deduce that the primary  $\alpha$ -phase was an FCC solid solution while the primary  $\beta$ -phase might be the Laves phase. The eutectic structure was a mixture of FCC and Laves phases, which was consistent with the results obtained for arc melting. This indicated that the different synthetic methods did not change the crystalline structure of the alloy.

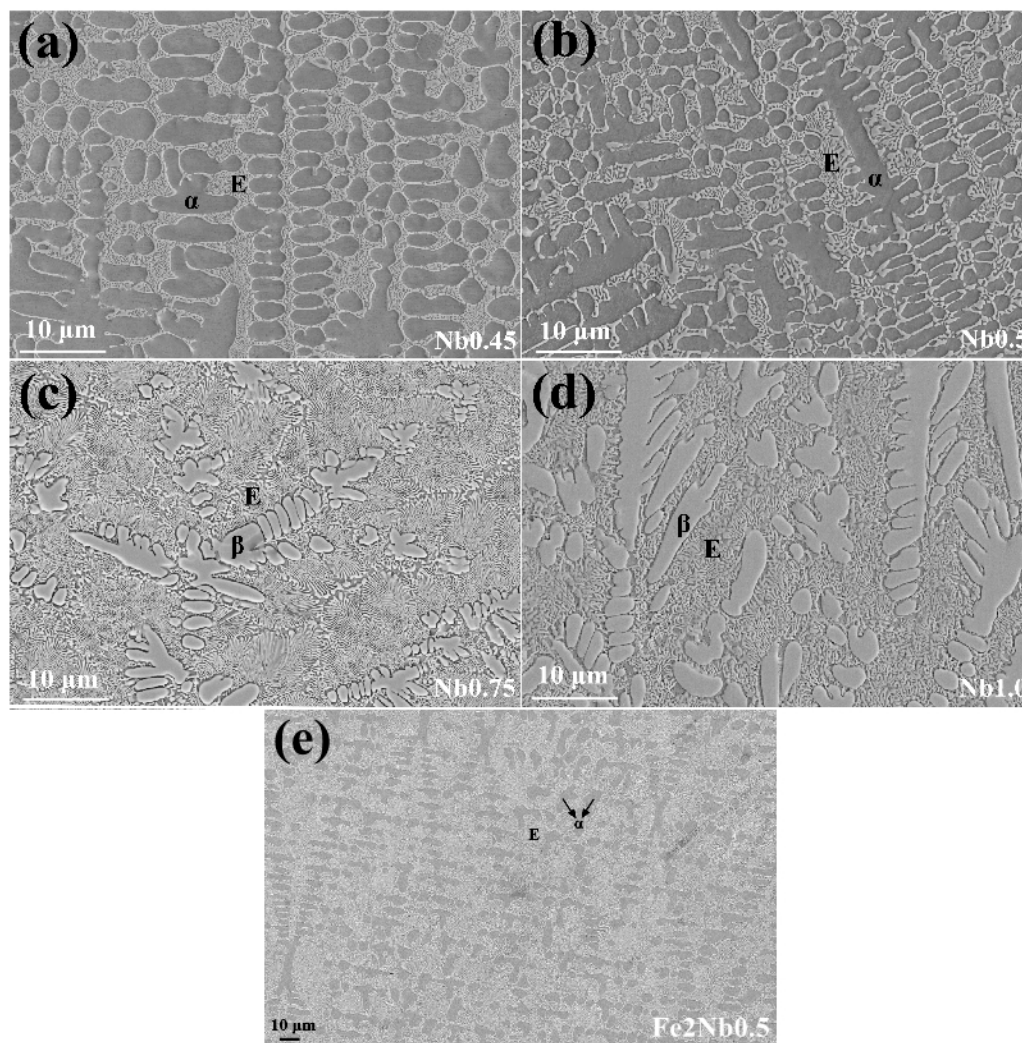


**Figure 3.** SEM images of the central area in the cladding zone of CoCrFeNiNb<sub>x</sub> HEA coatings (a) Nb0.45, (b) Nb0.5, (c) Nb0.75, (d) Nb1.0, (e) Fe2Nb0.5.

**Table 2.** Chemical compositions of CoCrFeNiNb<sub>x</sub> HEA coatings at the various regions (eutectic region is denoted by E) in Figure 3, given as atomic percentages.

Alloy	Regions	Co	Cr	Fe	Ni	Nb
Nb0.45	α	18.73	23.76	36.18	18.82	2.52
	E	18.29	19.33	28.03	17.65	16.71
Nb0.5	α	19.16	24.42	33.12	20.14	3.16
	E	18.69	20.72	27.03	18.83	14.73
Nb0.75	β	15.52	16.02	29.86	12.44	26.16
	E	15.51	19.84	31.66	15.52	17.47
Nb1.0	β	15.25	15.75	29.12	11.9	27.97
	E	15.16	21.47	33.21	17.02	13.14

### 3.3. Micro-Hardness of Coatings

Figure 4 presents a typical Vickers hardness profile of CoCrFeNiNb<sub>x</sub> HEA laser cladding coatings with different Nb contents. These measurements were made along a straight line from the top of the alloyed layer to the substrate. The effect of the Nb content on the hardness was determined. From the upper surface to the interface of the clad layer, the Vickers hardness value changed very little, which suggested a homogeneous distribution of the phase in the alloy coatings. From Nb0.45 to Nb1.0, the hardness values of these samples were significantly increased, and even reached 385–590 HV, which was 1.8–2.8 times higher than that of the substrate of 205 HV. Wherein, the hardness of Nb1.0 was higher than that of the Al<sub>x</sub>CoCrCuFeNi high-entropy alloys (<550 HV) [41] and the medium-entropy CoCrNi/boride metal matrix composite (467 HV) [42]. In addition, the hardness of the Nb1.0 alloy coating was higher than that of some already used industrial wear-resistant materials, such as high-manganese steel, alloy steel (ZG35Cr2Si1MnMoRE, 5Cr5MoV, ZG22Cr8NiMoTiRE) and Cast Iron. The increased hardness with the added Nb can be explained by the following two major reasons. One was the change of the microstructure of HEA coatings. From Sections 3.1 and 3.2, it could be found that the microstructure changed from a hypoeutectic structure to a hypereutectic structure, in which the eutectic structure was a mixture of an FCC solid solution phase and hard Laves phase. Since the Laves phase was harder than the FCC phase. The volume fraction of the Laves phase increased with increasing Nb content and thus enhanced the hardness of alloy coatings. Moreover, the eutectic microstructure with a very fine lamellar structure exhibited high hardness. Secondly, the atomic radius of Nb (1.47 Å) is much larger than those of Co, Cr, Fe, and Ni, which are 1.251, 1.249, 1.241, and 1.246 Å, respectively. The large atomic radius of Nb added to the CoCrFeNi alloy would lead to a larger lattice distortion and improve the solid solution strengthening effect. Thus, the Nb0.45, Nb0.5, Nb0.75, and Nb1.0 alloy coatings possessed high micro-hardness values.

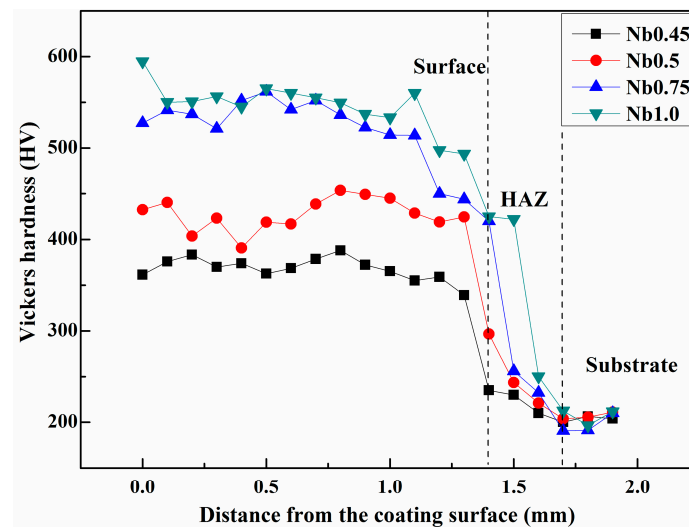


Figure 4. Micro-hardness from surface to substrate of all samples.

### 3.4. Wear Performance

It had been noted that the CoCrFeNiNb<sub>x</sub> HEA coatings with different Nb contents resulted in the improvement of the hardness value of the substrate. Therefore, these alloy coatings may show better wear resistance compared to the substrate. Usually, wear mass loss and depth/width of wear scar are used as the parameters to evaluate the wear resistance. Small wear mass loss and depth/width of wear scar represent good wear resistance. The wear mass loss of different alloy coatings is shown in Figure 5a. It was found that wear mass loss decreased with the increase of Nb content. The mass loss values in all of the HEA coatings were lower than that of the 304 stainless steel substrate. Among them, the wear mass loss of Nb1.0 alloy coating (1.4 mg) was less than one-third of that of the substrate (4.5 mg). The results showed Nb1.0 alloy coating possessed the highest wear resistance. Ten sets of wear tracks depth and width values were measured by a confocal laser scanning microscope (LEXT) after a sliding test. The average values of the wear scar depth and width are given in Figure 5b. It could be found that the width of wear scar exhibited a downward trend with the increase of Nb content. This was in agreement with the tendency of the weight loss after wear test. It also indicated that wear resistance of the HEA coatings was consistent with Khrushchov's conclusion in which the wear resistance of materials was, in general, proportional to their Vickers hardness [43]. A comparison of the width/depth of the grinding track and the weight loss indicated that the CoCrFeNiNb<sub>x</sub> HEA coatings showed better wear resistance than that of the 304 stainless steel substrate under the dry sliding condition. Among them, the CoCrFeNiNb<sub>1.0</sub> HEA coating presented the best wear resistance.

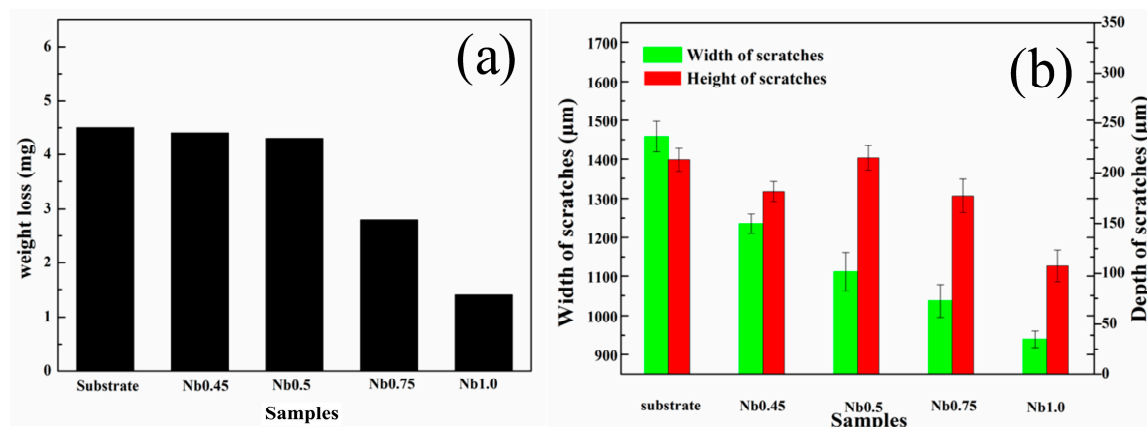
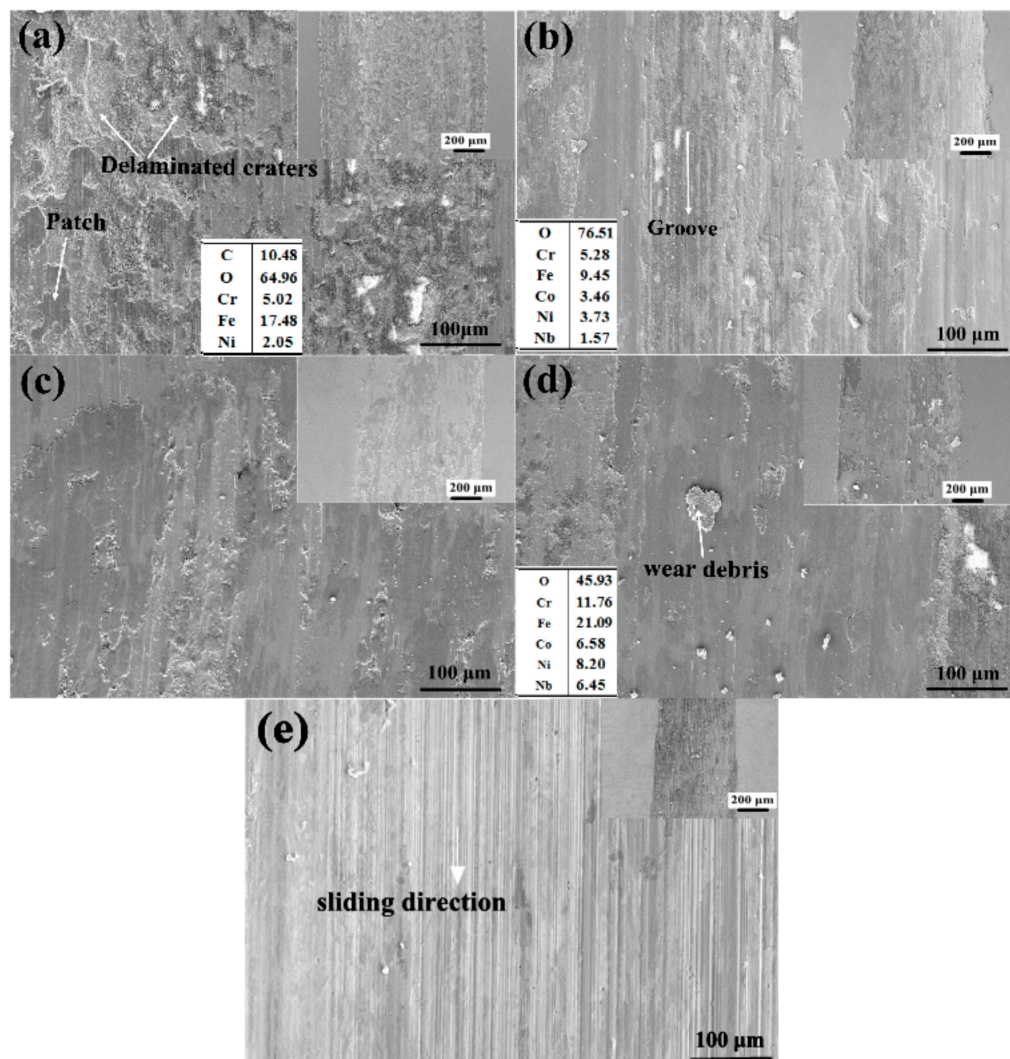


Figure 5. (a) Wear mass loss of all samples. (b) Depth and width of wear scars of the samples.

To understand the wear mechanism, it was critical to study the worn surface morphologies. Therefore, a detailed study of worn surfaces was performed using SEM, as shown in Figure 6. From the insert, it could be observed that widths of wear scars of the substrate were obviously wider than that of the CoCrFeNiNb<sub>x</sub> coatings with different Nb contents. With the increase of Nb content, the widths of wear scars of these coatings decreased. This indicated that wear resistance was improved by the laser surface alloying of CoCrFeNiNb<sub>x</sub> HEA on the 304 stainless steel. It was obvious that the extent of damage in the substrate sample was higher than the laser cladding coatings. The worn surface of the substrate showed that the whole contact interface presented the characteristics of obvious delaminated craters, large patches, and some white regions, see Figure 6a. The results of the EDS analysis indicated that the white region and the patches were highly enriched in oxygen, indicating that oxidation occurred on the worn surface. The formation of the oxide layer on the worn surface can result in cracking and the peeling-off of materials during dry sliding wear. This implied that there was a combination of adhesive wear, delaminated wear, and oxidative wear mechanisms. It was noted that as the hardness of the ceramic ball as a slider material was larger than that of substrate, this resulted in the transfer of substrate material to the ball surface in the initial stage of the wear test. As the sliding wear test continued, this transferred material may be oxidized during sliding and act as a three-body particle for abrasive wear [19]. The large amount of the alternate delaminated craters (which increases wear weight loss) and adhesive patches (which decrease wear weight loss) on the surface of the 304 stainless steel resulted in the increase in the wear rate. For the laser cladding coatings, the wear surface morphologies were different from the substrate, in which an adhesive wear feature did not clearly exist and they were relatively smoother with shallow grooves. It is noted that a number of shallow ploughed furrows coupled with plastic deformation along the groove, adhesive craters, and some wear debris appeared on the worn surface of Nb0.45 alloy coating shown in Figure 6b. The worn surfaces of the Nb0.5 and Nb0.75 alloy coatings were relatively smoother than the Nb0.45 alloy coating. Delaminated craters and plate-like wear debris also appeared on the worn surfaces. The EDS results showed that the wear debris contained a lot of oxygen, indicating the coating surface was oxidized. The formed oxide layer on the coating surface lead to the formation of shallow abrasive grooves during the sliding. The number of delaminated craters was lower than that in the substrate. Thus, these coatings preserved a lower wear rate than that of the substrate. It could be inferred that the wear mechanism for the Nb0.45, Nb0.5, and Nb0.75 HEA coatings was a combination of abrasive wear, oxidative wear, and delaminated wear. The wear surface of Nb1.0 alloy coating, see Figure 6e, showed a very smooth surface with fine wear tracks aligned in the sliding direction, which resulted from the high hardness. Meanwhile, the oxygen from the environment may play an important role during the wear process. When the chemically active elements (Nb and Fe) were contained in this region, a thin oxide layer formed quickly. The effective lubricating films formed on the sliding surface could escape from the contact regions; thus, reducing the wear of sample. It could be inferred that the wear mechanism for the Nb1.0 coating was a combination of abrasive wear and oxidative wear. These observations revealed that the Nb1.0 alloy possessed the best wear resistance among the tested samples. The improvement of the wear resistance might mainly be attributed to the proper combination of the high fracture toughness of FCC and the high hardness of Laves phases.





**Figure 6.** The SEM micrographs of worn surface of samples: (a) Substrate, (b) Nb0.45, (c) Nb0.5, (d) Nb0.75, and (e) Nb1.0. The insert is the EDS analysis result.

#### 4. Conclusions

High-quality CoCrFeNiNb<sub>x</sub> ( $x = 0.45, 0.5, 0.75, 1.0$ ) HEA coatings were successfully prepared by laser cladding on a 304 stainless steel substrate. It showed that the CoCrFeNiNb<sub>x</sub> HEA coatings were composed of a simple FCC solid solution and Laves phases. The volume fraction of hard Laves phase increased with increasing Nb content resulting in an increased hardness of the alloy coatings. The CoCrFeNiNb<sub>1.0</sub> alloy coating showed the highest hardness and best wear resistance property compared to other coatings and the substrate. The hardness value of CoCrFeNiNb<sub>1.0</sub> alloy coating was 2.8 times higher than that of the 304 stainless steel substrate. The wear mass loss of the CoCrFeNiNb<sub>1.0</sub> alloy coating was less than one-third of the substrate. The obvious improvement of the mechanical properties was considered with the fine lamellar eutectic structure and proper combination of FCC and Laves phases.

**Author Contributions:** The experiment was designed by H.J. The result analysis was performed by H.J. and K.H. D.L. conceived the investigation. H.J., K.H. and Z.C. were responsible for writing the paper.

**Funding:** This work was supported by the National Natural Science Foundation of China (Nos. 51671044, 51471044, 51525401 and 51574058), Dalian Support Plan for Innovation of High-level Talents (Top and Leading Talents, 2015R013), the Fundamental Research Funds for the Central Universities, and the National Key Research and Development Program of China (No. 2016YB0701203).

**Conflicts of Interest:** The authors declare no conflict of interest.



## References

1. Yeh, J.W.; Chen, S.K.; Lin, S.J.; Gan, J.Y.; Chin, T.S.; Shun, T.T.; Tsau, C.H.; Chang, S.Y. Nanostructured High-entropy alloys with multiple principal elements: Novel alloy design concepts and outcomes. *Adv. Eng. Mater.* **2004**, *6*, 299–303. [\[CrossRef\]](#)
2. Cantor, B.; Chang, I.T.H.; Knight, P.; Vincent, A.J.B. Microstructural development in equiatomic multicomponent alloys. *Mater. Sci. Eng. A* **2004**, *375–377*, 213–218. [\[CrossRef\]](#)
3. Zhang, Y.; Zuo, T.T.; Tang, Z.; Gao, M.C.; Dahmen, K.A.; Liaw, P.K.; Lu, Z.P. Microstructures and properties of high-entropy alloys. *Prog. Mater. Sci.* **2014**, *61*, 1–93. [\[CrossRef\]](#)
4. Gao, M.C.; Yeh, J.W.; Liaw, P.K.; Zhang, Y. Fundamentals and applications. In *High Entropy Alloys*; Springer: Berlin, Germany, 2016; p. 524.
5. Gludovatz, B.; Hohenwarter, A.; Catoor, D.; Chang, E.H.; George, E.P.; Ritchie, R.O. A fracture-resistant high-entropy alloy for cryogenic applications. *Science* **2014**, *345*, 1153–1158. [\[CrossRef\]](#) [\[PubMed\]](#)
6. Senkov, O.N.; Wilks, G.B.; Scott, J.M.; Miracle, D.B. Mechanical properties of Nb<sub>25</sub>Mo<sub>25</sub>Ta<sub>25</sub>W<sub>25</sub> and V<sub>20</sub>Nb<sub>20</sub>Mo<sub>20</sub>Ta<sub>20</sub>W<sub>20</sub> refractory high entropy alloys. *Intermetallics* **2011**, *19*, 698–706. [\[CrossRef\]](#)
7. Guo, N.N.; Wang, L.; Luo, L.S.; Li, X.Z.; Su, Y.Q.; Guo, J.J.; Fu, H.Z. Microstructure and mechanical properties of refractory MoNbHfZrTi high-entropy alloy. *Mater. Des.* **2015**, *81*, 87–94. [\[CrossRef\]](#)
8. Lilensten, L.; Couzinié, J.P.; Bourgon, J.; Perrière, L.; Dirras, G.; Prima, F.; Guillot, I. Design and tensile properties of a bcc Ti-rich high-entropy alloy with transformation-induced plasticity. *Mater. Res. Lett.* **2016**, *5*, 110–116. [\[CrossRef\]](#)
9. Sheikh, S.; Shafeie, S.; Hu, Q.; Ahlström, J.; Persson, C.; Veselý, J.; Zýka, J.; Klement, U.; Guo, S. Alloy design for intrinsically ductile refractory high-entropy alloys. *J. Appl. Phys.* **2016**, *120*, 164902. [\[CrossRef\]](#)
10. Zhao, Y.J.; Qiao, J.W.; Ma, S.G.; Gao, M.C.; Yang, H.J.; Chen, M.W.; Zhang, Y. A hexagonal close-packed high-entropy alloy: The effect of entropy. *Mater. Des.* **2016**, *96*, 10–15. [\[CrossRef\]](#)
11. Feuerbacher, M.; Heidelmann, M.; Thomas, C. Hexagonal high-entropy alloys. *Mater. Res. Lett.* **2014**, *3*, 1–6. [\[CrossRef\]](#)
12. Takeuchi, A.; Amiya, K.; Wada, T.; Yubuta, K.; Zhang, W. High-entropy alloys with a hexagonal close-packed structure designed by equi-atomic alloy strategy and binary phase diagrams. *JOM* **2014**, *66*, 1984–1992. [\[CrossRef\]](#)
13. Lilensten, L.; Couzinié, J.P.; Perrière, L.; Bourgon, J.; Emery, N.; Guillot, I. New structure in refractory high-entropy alloys. *Mater. Lett.* **2014**, *132*, 123–125. [\[CrossRef\]](#)
14. Chuang, M.H.; Tsai, M.H.; Tsai, C.W.; Yang, N.H.; Chang, S.Y.; Yeh, J.W.; Chen, S.K.; Lin, S.J. Intrinsic surface hardening and precipitation kinetics of Al<sub>0.3</sub>CrFe<sub>1.5</sub>MnNi<sub>0.5</sub> multi-component alloy. *J. Alloy Compd.* **2013**, *551*, 12–18. [\[CrossRef\]](#)
15. Dong, Y.; Gao, X.X.; Lu, Y.P.; Wang, T.; Li, T. A multi-component AlCrFe<sub>2</sub>Ni<sub>2</sub> alloy with excellent mechanical properties. *Mater. Lett.* **2016**, *169*, 62–64. [\[CrossRef\]](#)
16. Zhou, Y.J.; Zhang, Y.; Wang, Y.L.; Chen, G.L. Solid solution alloys of AlCoCrFeNiTi<sub>x</sub> with excellent room-temperature mechanical properties. *Appl. Phys. Lett.* **2007**, *90*, 181904. [\[CrossRef\]](#)
17. Chuang, M.H.; Tsai, M.H.; Wang, W.R.; Lin, S.J.; Yeh, J.W. Microstructure and wear behavior of Al<sub>x</sub>Co<sub>1.5</sub>CrFeNi<sub>1.5</sub>Ti<sub>y</sub> high-entropy alloys. *Acta. Mater.* **2011**, *59*, 6308–6317. [\[CrossRef\]](#)
18. Hsu, C.Y.; Yeh, J.W.; Chen, S.K.; Shun, T.T. Wear resistance and high-temperature compression strength of FCC CuCoNiCrAl<sub>0.5</sub>Fe alloy with boron addition. *Metall. Mater. Trans. A* **2004**, *35*, 1465–1469. [\[CrossRef\]](#)
19. Yu, Y.; Wang, J.; Li, J.; Yang, J.; Kou, H.; Liu, W. Tribological Behavior of AlCoCrFeNi(Ti<sub>0.5</sub>) high entropy alloys under oil and MACs lubrication. *J. Mater. Sci. Technol.* **2016**, *32*, 470–476. [\[CrossRef\]](#)
20. Daoud, H.M.; Manzoni, A.M.; Wanderka, N.; Glatzel, U. High-temperature tensile strength of Al<sub>10</sub>Co<sub>25</sub>Cr<sub>8</sub>Fe<sub>15</sub>Ni<sub>36</sub>Ti<sub>6</sub> compositionally complex alloy (high-entropy alloy). *JOM* **2015**, *67*, 2271–2277. [\[CrossRef\]](#)
21. He, F.; Wang, Z.; Shang, X.; Leng, C.; Li, J.; Wang, J. Stability of lamellar structures in CoCrFeNiNb<sub>x</sub> eutectic high entropy alloys at elevated temperatures. *Mater. Des.* **2016**, *104*, 259–264. [\[CrossRef\]](#)
22. Shi, Y.; Yang, B.; Liaw, P. Corrosion-resistant high-entropy alloys: A review. *Metal* **2017**, *7*, 43. [\[CrossRef\]](#)
23. Shi, Y.; Yang, B.; Xie, X.; Brechtel, J.; Dahmen, K.A.; Liaw, P.K. Corrosion of Al<sub>x</sub>CoCrFeNi high-entropy alloys: Al-content and potential scan-rate dependent pitting behavior. *Corros. Sci.* **2017**, *119*, 33–45. [\[CrossRef\]](#)

24. Kozelj, P.; Vrtnik, S.; Jelen, A.; Jazbec, S.; Jaglicic, Z.; Maiti, S.; Feuerbacher, M.; Steurer, W.; Dolinsek, J. Discovery of a superconducting high-entropy alloy. *Phys. Rev. Lett.* **2014**, *113*, 107001. [[CrossRef](#)] [[PubMed](#)]
25. Vrtnik, S.; Koželj, P.; Meden, A.; Maiti, S.; Steurer, W.; Feuerbacher, M.; Dolinšek, J. Superconductivity in thermally annealed Ta-Nb-Hf-Zr-Ti high-entropy alloys. *J. Alloy Compd.* **2017**, *695*, 3530–3540. [[CrossRef](#)]
26. Zhang, Y.; Zuo, T.; Cheng, Y.; Liaw, P.K. High-entropy alloys with high saturation magnetization, electrical resistivity, and malleability. *Sci. Rep.* **2013**, *3*, 1455. [[CrossRef](#)] [[PubMed](#)]
27. Lin, P.C.; Cheng, C.Y.; Yeh, J.W.; Chin, T.S. Soft magnetic properties of high-entropy Fe-Co-Ni-Cr-Al-Si thin films. *Entropy* **2016**, *18*, 308. [[CrossRef](#)]
28. Song, L.J.; Zeng, G.C.; Xiao, H.; Xiao, X.F.; Li, S.M. Repair of 304 stainless steel by laser cladding with 316L stainless steel powders followed by laser surface alloying with WC powders. *J. Manuf. Process.* **2016**, *24*, 116–124. [[CrossRef](#)]
29. Lv, Y.H.; Li, J.; Tao, Y.F.; Hu, L.F. Oxidation behaviors of the TiNi/Ti<sub>2</sub>Ni matrix composite coatings with different contents of TaC addition fabricated on Ti<sub>6</sub>Al<sub>4</sub>V by laser cladding. *J. Alloy Compd.* **2016**, *679*, 202–212. [[CrossRef](#)]
30. Zhang, C.; Chen, G.J.; Dai, P.Q. Evolution of the microstructure and properties of laser-clad FeCrNiCoBx high-entropy alloy coatings. *Mater. Sci. Technol.* **2016**, *32*, 1–7. [[CrossRef](#)]
31. Wu, C.L.; Zhang, S.; Zhang, C.H.; Zhang, H.; Dong, S.Y. Phase evolution and cavitation erosion-corrosion behavior of FeCoCrAlNiTi<sub>x</sub> high entropy alloy coatings on 304 stainless steel by laser surface alloying. *J. Alloy Compd.* **2017**, *698*, 761–770. [[CrossRef](#)]
32. Chen, S.; Chen, X.; Wang, L.; Liang, J.; Liu, C. Laser cladding FeCrCoNiTiAl high entropy alloy coatings reinforced with self-generated TiC particles. *J. Laser Appl.* **2017**, *29*, 012004. [[CrossRef](#)]
33. Zhang, S.; Wu, C.L.; Zhang, C.H.; Guan, M.; Tan, J.Z. Laser surface alloying of FeCoCrAlNi high-entropy alloy on 304 stainless steel to enhance corrosion and cavitation erosion resistance. *Opt. Laser Technol.* **2016**, *84*, 23–31. [[CrossRef](#)]
34. Zhang, H.; Pan, Y.; He, Y.Z.; Jiao, H.S. Microstructure and properties of 6FeNiCoSiCrAlTi high-entropy alloy coating prepared by laser cladding. *Appl. Surf. Sci.* **2011**, *257*, 2259–2263. [[CrossRef](#)]
35. Jiang, H.; Jiang, L.; Qiao, D.X.; Lu, Y.P.; Wang, T.M.; Cao, Z.Q.; Li, T.J. Effect of niobium on microstructure and properties of the CoCrFeNb<sub>x</sub>Ni high entropy alloys. *J. Mater. Sci. Technol.* **2017**, *33*, 712–717. [[CrossRef](#)]
36. Jiang, L.; Lu, Y.P.; Jiang, H.; Wang, T.M.; Wei, B.N.; Cao, Z.Q.; Li, T.J. Formation rules of single phase solid solution in high entropy alloys. *Mater. Sci. Technol.* **2015**, *32*, 588–592. [[CrossRef](#)]
37. Guo, S.; Ng, C.; Lu, J.; Liu, C.T. Effect of valence electron concentration on stability of fcc or bcc phase in high entropy alloys. *J. Appl. Phys.* **2011**, *109*, 103505. [[CrossRef](#)]
38. Wang, Z.; Huang, Y.; Yang, Y.; Wang, J.; Liu, C.T. Atomic-size effect and solid solubility of multicomponent alloys. *Scr. Mater.* **2015**, *94*, 28–31. [[CrossRef](#)]
39. Dong, Y.; Lu, Y.; Jiang, L.; Wang, T.; Li, T. Effects of electro-negativity on the stability of topologically close-packed phase in high entropy alloys. *Intermetallics* **2015**, *52*, 105–109. [[CrossRef](#)]
40. Liu, W.H.; Wu, Y.; He, J.Y.; Zhang, Y.; Liu, C.T.; Lu, Z.P. The phase competition and stability of high-entropy alloys. *JOM* **2014**, *66*, 1973–1983. [[CrossRef](#)]
41. Wu, J.M.; Lin, S.J.; Yeh, J.W.; Chen, S.K.; Huang, Y.S.; Chen, H.C. Adhesive wear behavior of Al<sub>x</sub>CoCrCuFeNi high-entropy alloys as a function of aluminum content. *Wear* **2006**, *261*, 513–519. [[CrossRef](#)]
42. Moravcik, I.; Gouvea, L.; Cupera, J.; Dlouhy, I. Preparation and properties of medium entropy CoCrNi/boride metal matrix composite. *J. Alloy Compd.* **2018**, *748*, 979–988. [[CrossRef](#)]
43. Hsu, C.Y.; Sheu, T.S.; Yeh, J.W.; Chen, S.K. Effect of iron content on wear behavior of AlCoCrFe<sub>x</sub>Mo<sub>0.5</sub>Ni high-entropy alloys. *Wear* **2010**, *268*, 653–659. [[CrossRef](#)]

